



# A tract-based diffusion study of cerebral white matter in neuromyelitis optica reveals widespread pathological alterations

Yaou Liu<sup>1</sup>, Yunyun Duan<sup>1</sup>, Yong He<sup>2</sup>, Chunshui Yu<sup>1</sup>, Jun Wang<sup>2</sup>, Jing Huang<sup>1</sup>, Jing Ye<sup>3</sup>, Helmut Butzkueven<sup>4</sup>, Kuncheng Li<sup>1</sup> and Ni Shu<sup>2</sup>

## Abstract

**Background:** It remains uncertain whether neuromyelitis optica (NMO) exhibits diffuse cerebral abnormalities or whether the pathology is truly restricted to optic nerves and spinal cord in the majority of cases. We examined NMO patients with diffusion tensor imaging (DTI) and utilized a tract-based spatial statistics (TBSS) method to analyze the data.

**Methods:** Twenty-seven NMO patients (25 females, age mean  $\pm$  SD: 35.1  $\pm$  12 years) and 27 age- and sex-matched normal controls were included in this study. Voxel-wise analyses were performed with TBSS using multiple diffusion metrics, including fractional anisotropy (FA), mean diffusivity (MD), axial diffusivity ( $\lambda_1$ ) and radial diffusivity ( $\lambda_{23}$ ).

**Results:** The NMO patients had significantly increased MD (3.6%),  $\lambda_1$  (2.6%) and  $\lambda_{23}$  (4.6%) in their white matter (WM) skeletons compared with the controls. Furthermore, TBSS analyses revealed significantly ( $p < 0.05$ , corrected for multiple comparisons) increased diffusivities (MD,  $\lambda_1$  and  $\lambda_{23}$ ) in many cerebral WM tracts in the patients with NMO, including the superior and inferior longitudinal fasciculi, inferior fronto-occipital fasciculi, corpus callosum, cingulum bundles, corticospinal tracts, optic radiation, uncinata fasciculi, fornices, internal capsules, external capsules and cerebral peduncles. Exploratory analyses also revealed the possible associations between WM diffusion changes (MD,  $\lambda_1$  and  $\lambda_{23}$ ) and clinical variables (Expanded Disability Status Scale and disease duration) in the patients.

**Conclusions:** This study provided imaging evidence for widespread cerebral WM abnormalities. While these findings require independent replication, they potentially signify the presence of widespread, low-grade cerebral pathology in NMO.

## Keywords

neuromyelitis optica; diffusion tensor imaging; tract-based spatial statistics

Date received: 31st August 2011; revised: 1st November 2011; accepted: 7th November 2011

## Introduction

Neuromyelitis optica (NMO; or Devic's disease) is an auto-immune inflammatory disease of the central nervous system. This syndrome is clinically characterized by recurrent attacks of optic neuritis and myelitis.<sup>1,2</sup> Currently, it remains uncertain whether NMO exhibits diffuse cerebral abnormalities or whether the pathology is truly restricted to optic nerves and spinal cord in the majority of cases.<sup>3–8</sup>

Diffusion tensor imaging (DTI) can be used to regionally quantify the micro-structural integrity of white matter (WM) tracts. Fractional anisotropy (FA) and mean diffusivity (MD) are commonly used diffusion metrics in studies of brain diseases,<sup>9,10</sup> and these are believed to provide a general, non-specific measure of tissue alteration. More recently, the directional diffusivity measures axial diffusivity,  $\lambda_1$ , and radial diffusivity,  $\lambda_{23}$ , of WM tracts have been proposed to differentiate between axonal injury and demyelination to some extent, although the

large number of pathological alterations in diseased human WM limit their interpretation.<sup>11–15</sup>

<sup>1</sup>Department of Radiology, Xuanwu Hospital, Capital Medical University, Beijing, China.

<sup>2</sup>State Key Laboratory of Cognitive Neuroscience and Learning, Beijing Normal University, Beijing, China.

<sup>3</sup>Department of Neurology, Xuanwu Hospital, Capital Medical University, Beijing, China.

<sup>4</sup>Department of Medicine, University of Melbourne, Parkville, Australia.

### Corresponding authors:

Ni Shu, PhD, State Key Laboratory of Cognitive Neuroscience and Learning, Beijing Normal University, Beijing 100875, China.  
Email: nshu55@gmail.com

Kuncheng Li, MD, Department of Radiology, Xuanwu Hospital, Capital Medical University, Beijing 100053, China.  
Email: kunchengli55@gmail.com

**Table 1.** Demographics of participants .

	NMO (n = 27)	Controls (n = 27)	p-values
Mean age (range) [years]	35.1 (19–59)	34.2 (19–52)	0.77
Sex (M/F)	2/25	2/25	>0.99
Median EDSS (range)	3.6 (1.0-6.0)	–	–
Mean disease duration (range) [months]	56 (6-240)	–	–
Mean ON events (SD)	1.9 (1.6)	–	–
Mean myelitis events (SD)	2.1 (1.5)	–	–
Progression index (SD)	0.6 (1.1)	–	–
Annualized relapse rate (SD)	0.9 (1.2)	–	–

Abbreviations: NMO, neuromyelitis optica; EDSS, Expanded Disability Status Scale; ON, optic neuritis.

Several previous DTI studies have utilized diffusion metrics to investigate potential changes in normal appearing white matter (NAWM) in patients with NMO, with discordant results. Rocca and colleagues<sup>8</sup> examined the extent of mean diffusivity histogram-derived metrics of NAWM in NMO patients and controls, and found that there were no significant differences between the groups. However, studies from our group<sup>6,7</sup> showed that NMO patients had a higher mean diffusivity in NAWM than the controls. Using region-of-interest (ROI) and tractography-based quantitative analyses, we further showed that NMO patients had abnormal diffusion measures in corticospinal tracts and optic radiations. However, secondary degeneration of these tracts would be expected in patients with severe optic neuritis and spinal cord pathology, and thus do not provide evidence for more widespread non-lesional cerebral pathology in NMO.

The tract-based spatial statistics (TBSS) method is a recently developed, fully automated whole-brain analysis technique that applies voxel-wise statistics to diffusion measures. Its particular advantage is that it minimizes the effects of tract misalignment encountered by conventional voxel-based analysis methods, which use templates derived from health controls, leading to systematic misalignments in patients with pathological atrophy.<sup>16</sup> To circumvent this problem, the TBSS method extracts each subject's WM skeleton (i.e. the center of all major tracts 'common' to all subjects) from the normalized FA images, thus minimizing the effect of atrophy-induced misregistration. This method is now increasingly used in studies characterizing WM abnormalities in various brain diseases, such as Alzheimer's disease<sup>10</sup>, schizophrenia<sup>17,18</sup> and multiple sclerosis (MS).<sup>19</sup>

Our study is the first to apply the TBSS technique to the investigation of cerebral abnormalities in NMO. In this study, we utilized the TBSS method to more accurately localize multiple diffusion metrics (FA, MD,  $\lambda_1$  and  $\lambda_{23}$ ) in cerebral WM. After characterizing widespread diffusion abnormalities in cerebral NAWM in NMO, we next

investigated the correlations between the identified NAWM abnormalities and clinical characteristics.

## Subjects and methods

### Participants

Twenty-five female and two male NMO patients (mean age  $\pm$  SD: 35.1  $\pm$  12 years) and 27 age- and gender-matched normal controls (NC; mean age  $\pm$  SD: 34.2  $\pm$  10.6 years) participated in this study. The diagnosis of NMO was made by an experienced neurologist with special expertise in WM disease, Dr Jing Ye. All patients fulfilled the recently revised diagnostic criteria for NMO.<sup>1</sup> As NMO IgG testing was not available, all patients met both the absolute criteria, namely episodes of optic neuritis and myelitis, as well as the supporting criteria of brain MRI results that were negative or non-diagnostic for MS, and MRI evidence of a longitudinally extensive spinal cord T2 lesion spanning at least three vertebral segments. The disability scores of all patients were assessed using Kurtzke's Expanded Disability Status Scale (EDSS).<sup>20</sup> The patients' EDSS scores ranged from 1.0 to 6.0, indicating that all patients could walk at least 100 m with a single-point stick. Table 1 presents the main demographic and clinical characteristics of the study participants, all of whom had relapsing NMO. Twenty-one patients had no T2 WM lesions on brain MRIs and six of them had small, non-specific WM lesions. None of the participating patients had been treated with disease-modifying medications (e.g. corticosteroids or immunosuppressive drugs) within 3 months before acquiring the MRI images. The normal controls had no history of neurological illness, no abnormal findings on neurological examination and no abnormalities detected with conventional brain MRI.

Different DTI data, using ROI and DTI histogram methods, from 13 of these patients were published before by our group.<sup>6,7</sup> The study was approved by the institutional review

board of Xuanwu Hospital and written informed consent was obtained from each participant.

### Data acquisition

All participants were scanned with a 1.5-T MR unit (Sonata, Siemens Medical Systems, Erlangen, Germany). The T2, T1 and DTI images were acquired using the following sequences: (a) T2-weighted turbo spin echo imaging [repetition time (TR)/echo time (TE) = 5460/94 ms; number of excitation (NEX) = 3; echo train length = 11; matrix = 224 × 256; field of view (FOV) = 210 mm × 240 mm; number of slices = 30; slice thickness = 4 mm; orientation = axial], (b) T1-weighted spin echo imaging [TR/TE = 1900/4 ms; NEX = 1; matrix = 224 × 256; FOV = 220 mm × 250 mm; number of slices = 96; slice thickness = 1.7 mm; orientation = sagittal] and (c) spin-echo single-shot echo planar imaging (EPI) [TR/TE = 5000/100 ms; NEX = 10; matrix = 128 × 128; FOV = 240 mm × 240 mm; number of slices = 30; slice thickness = 4 mm; slice gap = 0.4 mm; orientation = axial; six nonlinear diffusion weighting gradient directions with  $b = 1000$  s/mm<sup>2</sup> and one additional image without diffusion weighting (i.e.  $b = 0$  s/mm<sup>2</sup>)].

### Data preprocessing

DTI data was preprocessed using FMRIB's Diffusion Toolbox (FDT; FSL 4.1.4, www.fmrib.ox.ac.uk/fsl). First, eddy current distortions and motion artifacts in the DTI dataset were corrected by applying the affine alignment of each diffusion-weighted image to the  $b_0$  image. Then, the first volume of the diffusion data, without a gradient applied (i.e.  $b = 0$ ), was used to generate a binary brain mask with the Brain Extraction Tool. Finally, DTIfit was used to independently fit a diffusion tensor to each voxel. The output of DTIfit yielded voxel-wise maps of FA, MD,  $\lambda_1$  and  $\lambda_{23}$  for each subject. The FA, MD and  $\lambda_{23}$  of each voxel were calculated according to the following formulas:

$$FA = \frac{\sqrt{(\lambda_1 - \lambda_2)^2 + (\lambda_1 - \lambda_3)^2 + (\lambda_2 - \lambda_3)^2}}{\sqrt{2(\lambda_1^2 + \lambda_2^2 + \lambda_3^2)}} \quad (1)$$

$$MD = \frac{\lambda_1 + \lambda_2 + \lambda_3}{3} \quad (2)$$

$$\lambda_{23} = \frac{\lambda_2 + \lambda_3}{2} \quad (3)$$

### TBSS

The TBSS analyses of FA, MD,  $\lambda_1$  and  $\lambda_{23}$  images were carried out using the FMRIB software library (FSL 4.1.4; www.fmrib.ox.ac.uk/fsl); for a detailed description of the methods, see Smith et al.<sup>16</sup> Briefly, first we performed the

following five-step process on the FA images: (i) the FA image of each subject was aligned to a pre-identified target FA image (FMRIB58\_FA) by nonlinear registration; (ii) all of the aligned FA images were transformed into the MNI152 template by affine registration; (iii) the mean FA image and its skeleton (mean FA skeleton) were created from the images of all the subjects; (iv) individual subjects' FA images were projected onto the skeleton; (v) voxel-wise statistics across subjects were calculated for each point on the common skeleton. Then, data for MD,  $\lambda_1$  and  $\lambda_{23}$  were generated by applying the above FA transformations to additional diffusivity maps and projecting them onto the skeleton with projection vectors that were identical to the vectors inferred from the original FA data.

### Atlas-based quantification at the tract level

In order to investigate the diffusion changes in several specific tracts, we used the digital WM atlas JHU ICBM-DTI-81 (see <http://cmrm.med.jhmi.edu/>), which is a probabilistic atlas generated by mapping DTI data of 81 subject to a template image. It has discrete labeling from 0 to 50, representing different WM tracts. As shown in Figure 1A, the JHU WM atlas was overlaid on the WM skeleton of each subject in the ICBM-DTI-81 space, such that each skeleton voxel could be categorized into one of the major tracts. Then the mean diffusion metrics of the skeleton voxels within each tract can be calculated. We examined the following tracts: the genu, body and splenium of the corpus callosum, the bilateral cingulum bundles, the optic radiations and the corticospinal tracts (anterior and posterior limbs of internal capsule).

### Statistical analyses

First, we calculated the mean diffusion metrics (FA, MD,  $\lambda_1$  and  $\lambda_{23}$ ) in the whole-brain WM skeleton and in the atlas-based tract ROIs for each subject. Linear regression analyses were performed to compare the mean diffusion metrics between the NMO and NC groups. Age was treated as a covariate in the regression analysis. Owing to the small sample size and the preliminary nature of this study, we did not control for multiple comparisons for the atlas-based analyses.

Second, voxel-wise statistics in TBSS were carried out using a permutation-based inference tool for nonparametric statistical thresholding (the 'randomize' tool, part of FSL).<sup>16</sup> In this study, voxel-wise group comparisons were performed using non-parametric, two-sample  $t$ -tests between the NMO and NC groups, controlling for age. The mean FA skeleton was used as a mask (thresholded at a mean FA value of 0.2), and the number of permutations was set to 5000. The significance threshold for between-group differences was set at  $p < 0.05$  [family-wise error (FWE) corrected for multiple comparisons] using the threshold-free cluster enhancement (TFCE) option in the 'randomize'

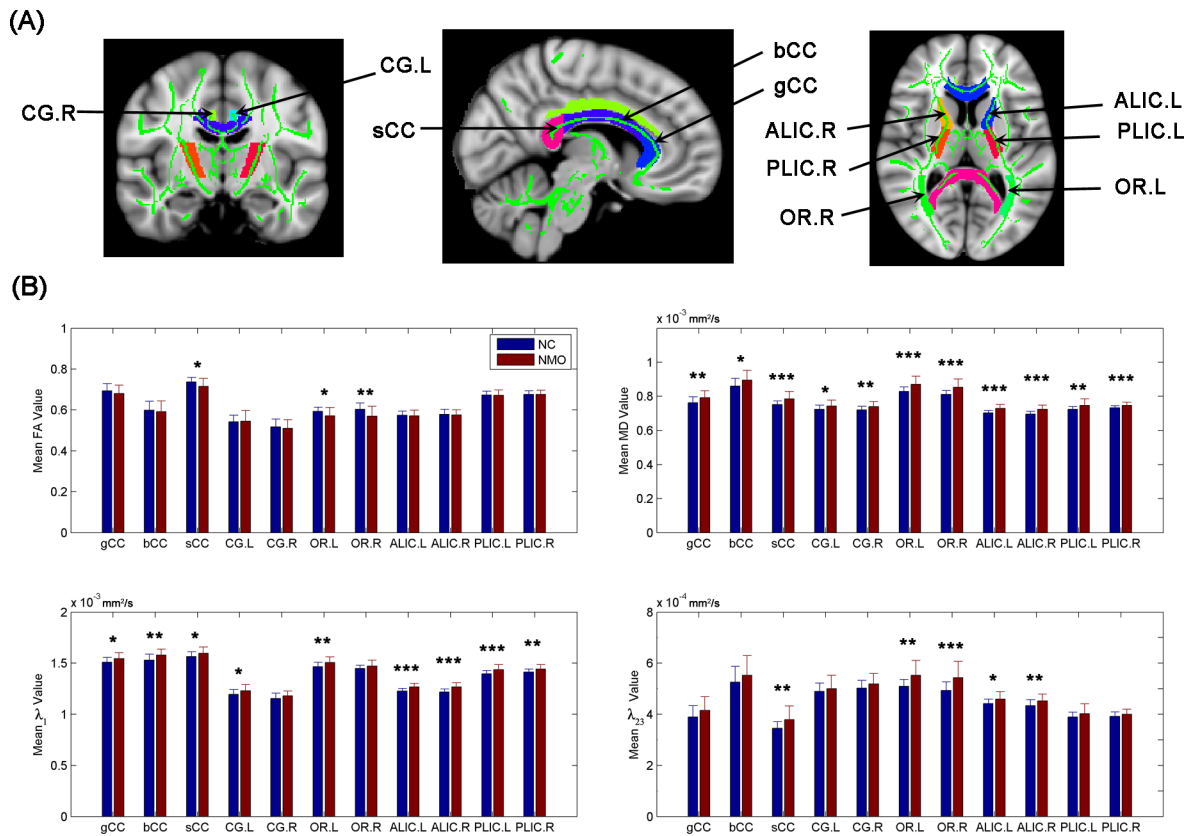


**Figure 1.** Mean diffusion metrics of the atlas-based tracts in normal controls (NC) and neuromyelitis optica (NMO) groups. (A) The JHU white matter (WM) atlas was overlaid on the mean WM skeleton in the ICBM-DTI-81 space. Colored regions indicate major WM tracts. The skeleton from averaged FA maps is shown as a green solid curve. ALIC, anterior limb of internal capsule; bCC, body of corpus callosum; CG, cingulum bundle at cingulate gyrus; gCC, genu of corpus callosum; OR: optic radiation; PLIC, posterior limb of internal capsule; sCC, splenium of corpus callosum. (B) Mean diffusion metrics and group differences of the each atlas-based tract in NC and NMO groups. \* $p < 0.05$ ; \*\* $p < 0.01$ ; \*\*\* $p < 0.001$ .

permutation-testing tool in FSL. Similarly, group comparisons of MD,  $\lambda_1$  and  $\lambda_{23}$  images were performed.

In addition, for the NMO patients, inter-subject voxel-wise correlations between each diffusion metric (FA, MD,  $\lambda_1$  and  $\lambda_{23}$ ) and EDSS scores were performed within a mask of the area, which is constrained in regions with significant group differences for each diffusion metric. Similar correlations between the voxel diffusion metrics and disease duration were also performed. We used a non-parametric, linear regression model to perform correlation analyses, treating age as a covariate. In an exploratory analysis, the significance threshold for correlations was set at  $p < 0.01$  (uncorrected) using the TFCE option in the 'randomize' permutation-testing tool in FSL.

## Results

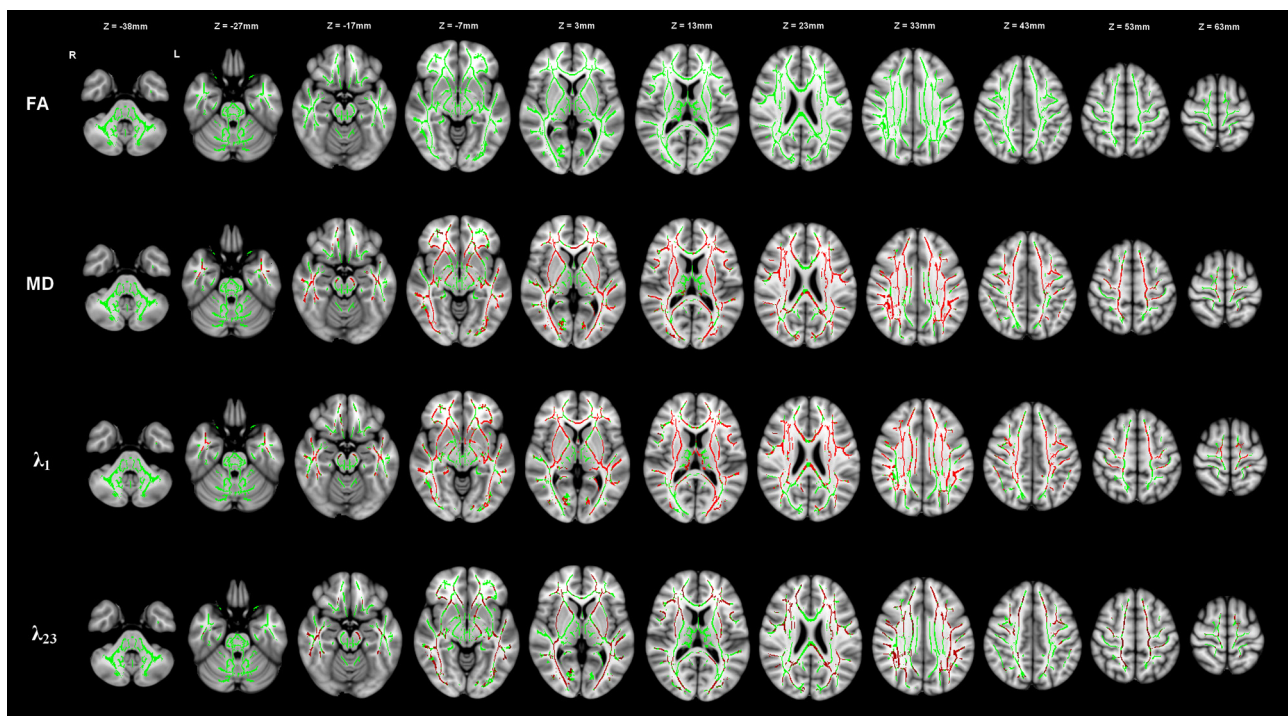
The mean diffusion measures FA, MD,  $\lambda_1$  and  $\lambda_{23}$  in the WM skeleton were extracted for each subject. Statistical analyses revealed significant between-group increases in MD [NMO (mean  $\pm$  SD):  $(7.97 \pm 0.29) \times 10^{-4}$  mm<sup>2</sup>/s; NC (mean  $\pm$  SD):  $(7.70 \pm 0.15) \times 10^{-4}$  mm<sup>2</sup>/s;  $t(51) = -4.54$ ,

$p = 3.5 \times 10^{-5}$ ],  $\lambda_1$  [NMO (mean  $\pm$  SD):  $(1.19 \pm 0.02) \times 10^{-3}$  mm<sup>2</sup>/s; NC (mean  $\pm$  SD):  $(1.16 \pm 0.02) \times 10^{-3}$  mm<sup>2</sup>/s;  $t(51) = -5.60$ ,  $p = 8.6 \times 10^{-7}$ ] and  $\lambda_{23}$  [NMO (mean  $\pm$  SD):  $(5.99 \pm 0.34) \times 10^{-4}$  mm<sup>2</sup>/s; NC (mean  $\pm$  SD):  $(5.73 \pm 0.17) \times 10^{-4}$  mm<sup>2</sup>/s;  $t(51) = -3.66$ ,  $p = 0.0006$ ] in the skeleton. There was a non-significant trend for a decrease in mean FA values between the two groups [NMO (mean  $\pm$  SD):  $0.42 \pm 0.02$ ; NC (mean  $\pm$  SD):  $0.43 \pm 0.01$ ;  $t(51) = 1.81$ ,  $p = 0.076$ ]. The NMO patients had significantly increased MD (3.6%),  $\lambda_1$  (2.6%) and  $\lambda_{23}$  (4.6%) in the cerebral WM skeletons compared with the controls.

Tract-based TBSS analyses revealed significantly increased MD,  $\lambda_1$  and  $\lambda_{23}$  in many WM tracts in NMO patients compared with healthy controls, including the bilateral superior longitudinal fasciculi (SLF), inferior longitudinal fasciculi (ILF), inferior fronto-occipital fasciculi (IFOF), corticospinal tracts (CST), optic radiations (OR), corpus callosum, cingulum bundles, uncinate fasciculi, fornices, internal capsules, external capsules and cerebral peduncles ( $p < 0.05$ , FWE corrected for multiple comparisons, see Table 2 and Figure 2). There were no significant tract specific FA differences between the two groups at

**Table 2.** Diffusion changes in the white matter tracts in neuromyelitis optica patients ( $p < 0.05$ , FWE corrected).

White matter tracts	MD	$\lambda_1$	$\lambda_{23}$
Superior longitudinal fasciculus	Bilateral	Bilateral	Bilateral
Inferior longitudinal fasciculus	Bilateral	Bilateral	Bilateral
Inferior fronto-occipital fasciculus	Bilateral	Bilateral	Bilateral
Corpus callosum	Genu and splenium	Genu, body and splenium	Genu and splenium
Cingulum bundles	Bilateral	Bilateral	–
Corticospinal tracts	Bilateral	Bilateral	Bilateral
Optic radiation	Bilateral	–	Bilateral
Uncinate fasciculus	Bilateral	Bilateral	Bilateral
Fornix	–	Bilateral	–
Anterior limb of internal capsule	Bilateral	Bilateral	Bilateral
Posterior limb of internal capsule	Bilateral	Bilateral	Left
External capsule	Bilateral	Bilateral	Bilateral
Cerebral peduncle	Bilateral	Bilateral	Left

**Figure 2.** Tract-based spatial statistics (TBSS) results of fractional anisotropy (FA), mean diffusivity (MD),  $\lambda_1$  and  $\lambda_{23}$  images between the normal controls (NC) and neuromyelitis optica (NMO) groups. Green represents the mean white matter skeleton of all subjects; red represents regions with increased MD, increased  $\lambda_1$  and increased  $\lambda_{23}$  in NMO patients ( $p < 0.05$ , FWE corrected for multiple comparisons).

$p < 0.05$  (FWE corrected for multiple comparisons). In order to fully account for the potential effect of non-specific WM lesions, we identified and excluded the six patients with small, non-specific cerebral WM lesions. Results were not significantly different to those including all patients (data not shown), which confirmed that the abnormal diffusivity changes were related to NAWM changes caused by NMO.

In addition, atlas-based tract analyses revealed reduced FA in the splenium of the corpus callosum and bilateral ORs, increased MD in the whole corpus callosum, bilateral cingulum bundles, ORs and anterior and posterior limbs of internal capsule, increased  $\lambda_1$  in the whole corpus callosum, left cingulum bundle, left OR and bilateral anterior and posterior limbs of internal capsule, increased  $\lambda_{23}$  in the

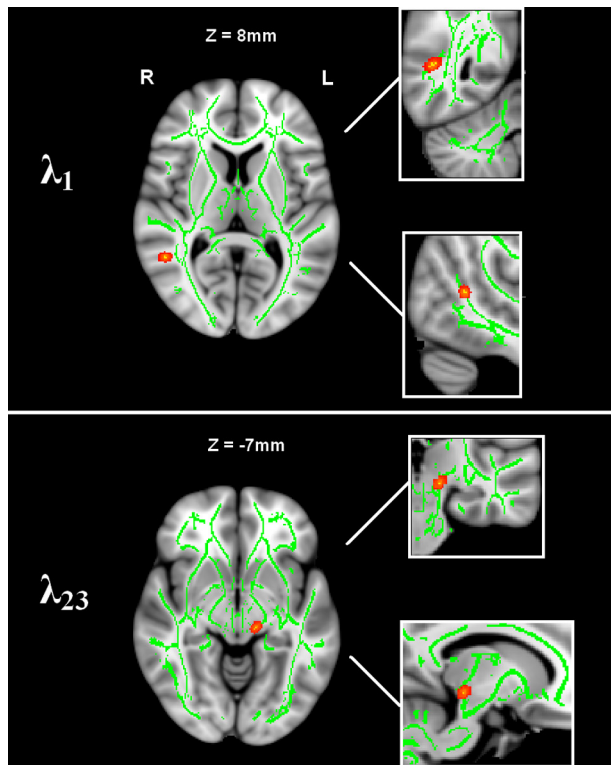


**Figure 3.** Tract-based spatial statistics (TBSS) results from linear regression analysis showing voxels (in red–yellow, thickened for better visibility) where an increase in Expanded Disability Status Scale scores was correlated with a  $\lambda_1$  increase (top) and a  $\lambda_{23}$  increase (bottom) ( $p < 0.01$ , uncorrected). Green represents the mean white matter skeleton of all the participants.

splenium of the corpus callosum, bilateral ORs and anterior limbs of internal capsule (Figure 1B).

In exploratory analyses, we found positive correlations ( $p < 0.01$ , uncorrected) between skeletal voxel  $\lambda_1$  and EDSS score in the middle part of the SLF, and between skeletal voxel  $\lambda_{23}$  and EDSS score in the corticospinal tract (Figure 3). There were no significant voxel-wise correlations between MD values and EDSS scores. Moreover, we found positive correlations ( $p < 0.01$ , uncorrected) between skeletal voxel MD and disease duration in several brain regions, including the WM of left anterior temporal lobe, left cerebral peduncle, bilateral occipital cortices, bilateral postcentral gyri (PoCG), right supplementary motor cortices (SMA) and left IFOF. Positive correlations between skeletal voxel  $\lambda_1$  and disease duration were found in the WM of the right temporal pole, left middle temporal gyrus and right IFOF. Positive correlations between skeletal voxel  $\lambda_{23}$  and disease duration were mainly located in the WM of the left fusiform cortex, right lingual gyrus, left middle temporal gyrus, bilateral PoCG and left IFOF (Figure 4). These results collectively suggest that NAWM diffusion abnormalities accumulate with increasing EDSS scores and increasing disease duration in NMO patients, although

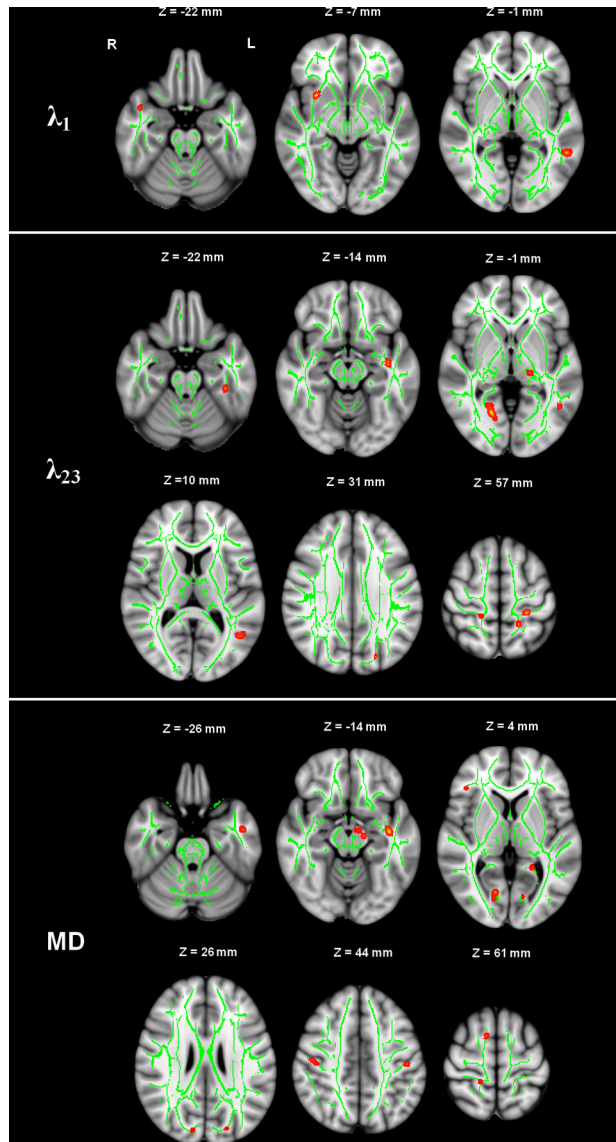


**Figure 4.** Tract-based spatial statistics (TBSS) results from linear regression analysis showing voxels (in red–yellow, thickened for better visibility) where an increase in disease duration was correlated with a  $\lambda_1$  increase (top), a  $\lambda_{23}$  increase (middle) and a mean diffusivity (MD) increase (bottom) ( $p < 0.01$ , uncorrected). Green represents the mean white matter skeleton of all of the participants.

none of above correlations between skeletal voxel diffusivity and EDSS scores or disease durations remained significant after correction for multiple testing ( $p < 0.05$ ), potentially a function of the modest sample size and large number of potentially correlated regions.

## Discussion

In this study, we investigated global WM changes in NMO patients by measuring FA, MD,  $\lambda_1$  and  $\lambda_{23}$  across the whole brain, using the patient-derived tract localization technique

TBSS. Compared with the controls, the NMO patients exhibited significantly increased  $\lambda_1$ ,  $\lambda_{23}$  and MD, and a trend towards decreased FA in many WM tracts, as described. This study may provide evidence for widespread, subtle cerebral WM changes in NMO.

In our study, nearly all of the WM tracts exhibited abnormal diffusion changes in NMO patients revealed by TBSS. Confirmatory, atlas-based tract analyses also showed diffusion abnormalities in specific WM tracts beyond the CST and OR, including the whole corpus callosum and bilateral cingulum bundles, which confirmed our TBSS findings. The discordances with previous studies<sup>6,7</sup> which only show CST and OR abnormalities are likely due to the increased sensitivity of the TBSS method and due to increased sample size. These findings indeed suggest that there are widespread structural changes in NAWM in NMO patients. The lack of specificity for visual or corticospinal tracts suggests that more complex mechanisms other than only trans-synaptic degeneration produce the abnormalities revealed in the current study. Concordant with the notion that subtle NMO pathology could extend into cerebral NAWM, a recent study evaluating neuropsychological tests in NMO patients revealed evidence of disease-associated cognitive impairment.<sup>21</sup>

It is believed that anti-aquaporin 4 antibodies contribute to pathogenesis,<sup>22,23</sup> and the aquaporin-4 water channel is widely expressed on astrocytes, including cerebral astrocytes. In concordance with this hypothesis, recent pathological descriptions strongly suggest that the primary cellular target of autoimmune CNS injury in NMO lesions are astrocytes<sup>24</sup> and a Japanese study confirmed marked CSF increase of the astrocytic protein GFAP in NMO relapses.<sup>25</sup> As the astrocyte, the presumed cellular target of NMO autoimmunity, is distributed across the brain and spinal cord, the confirmation of subtle, widespread diffusion abnormalities by DTI would suggest that NMO pathology could extend into the NAWM of the brain. Our study found trends towards correlations between disease duration and the extent of diffusion abnormalities, suggesting a possible evolution of pathology from lesion-restricted and intense to widespread in the NAWM and low grade. Other possible explanations for NAWM abnormalities in NMO include occult NAWM lesions which cannot be detected by current conventional MRI techniques or pathological consequences from cortical abnormalities reported previously.<sup>8</sup>

### Neural substrates of diffusion changes

Compared with the healthy controls, the NMO patients showed significantly increased MD,  $\lambda_1$  and  $\lambda_{23}$  in many brain regions by TBSS, but only a trend towards significantly decreased FA. These differential changes in diffusion metrics could provide some clues to the nature of the micro-structural changes in the WM.

Many studies of CNS neurological diseases have observed regional reductions in diffusion anisotropy, and

some researchers have proposed that the primary determinant of anisotropy is the packing density of axons within a voxel.<sup>26,27</sup> Axonal packing density encompasses a variety of micro-structural level variables (e.g. degree of myelination, axonal diameters, and extracellular space). As this study did not find significant changes in FA, however, significantly increase in MD,  $\lambda_1$  and  $\lambda_{23}$ . It may imply that FA, as a relative index, was not sensitive when the  $\lambda_1$  and  $\lambda_{23}$  changed proportionally. Therefore, the analysis of component eigenvalues was necessary to capture the full extent of WM changes. Selective decreased  $\lambda_1$  could reflect acute axonal loss or damage,<sup>12,13,28</sup> and selective increased  $\lambda_{23}$  could suggest predominant demyelination and a loss of myelin integrity.<sup>12,29</sup> Our findings, indicating a proportional increase in both component eigenvalues, are not pathologically specific and could reflect numerous subtle tissue alterations secondary to fibre re-organization, increase in membrane permeability, destruction of intracellular compartments, glial alterations,<sup>6,10,23</sup> axonal loss and increased axonal diameter,<sup>23</sup> all of which can induce water molecules to diffuse faster in unanticipated directions, accounting for increased  $\lambda_1$ .

In the NMO patients, we found most WM tracts had subtle increases in both  $\lambda_1$  and  $\lambda_{23}$ , which we interpret as definite but subtle tissue change. The increase in both  $\lambda_1$  and  $\lambda_{23}$  are also reported in some studies of pre-term infants,<sup>30</sup> normal aging,<sup>31</sup> and Alzheimer's disease,<sup>10</sup> all of which cause relatively low-grade alterations in WM. We speculate that, in NMO, the observed concomitant increases in MD and in both  $\lambda_1$  and  $\lambda_{23}$  could be due to low-grade astrocytic pathology, perhaps a small alteration in intracellular water content or increased reactivity secondary to sub-lethal antibody-mediated cellular injury. In this regard, MRI examination of appropriate animal models of NMO, which are being developed at present, could allow histological/DTI correlation studies to be performed to confirm or refute this hypothesis.

### Clinical correlations

A trend towards a positive correlation between EDSS and  $\lambda_{23}$  increase in the CST were identified in our study. The EDSS is predominantly a measure of motor function, particularly above EDSS score of 3.5.<sup>20</sup> The CST is the motor pathway that connects the cerebral motor cortex with the lateral motor tracts of the spinal cord. The SLF, as the main association fiber tract connecting the frontal, parietal and temporal lobes, plays an important role in regulating motor behavior.<sup>32</sup> Thus, the trend towards positive correlations between EDSS and CST/SLF diffusion abnormalities are not surprising, and could correspond to direct and trans-synaptic axonal degeneration following spinal cord lesions, but this will require confirmation in a replication dataset.

Our study also found a trend towards a positive correlation between disease duration and the extent of diffusion

abnormalities, suggesting a possible evolution of pathology from lesion-restricted and intense to widespread in the NAWM and low grade.

These results may collectively suggest that NAWM diffusion abnormalities accumulate with increasing EDSS scores and increasing disease duration in NMO patients, although none of above correlations between skeletal voxel diffusivity and EDSS scores or disease durations remained after correction for multiple testing ( $p < 0.05$ ).

### Limitations

The present study used a 4-mm slice thickness with a slice gap of 0.4 mm for the DTI data and a suboptimal DTI sequence with six diffusion-encoding gradient directions. In the TBSS analyses, the DTI data were converted into MNI space with an isotropic resolution of  $1 \text{ mm} \times 1 \text{ mm} \times 1 \text{ mm}$ . Therefore, all of the clusters with diffusion changes in patients detected in this study were more than 4 mm in length, as diffusion changes less than 4 mm in the  $z$ -axis direction could not be reliably evaluated due to the resolution limit. Moreover, it should be noted that the sequence with six gradient directions could provide different metrics than sequences with a higher number of diffusion axes; particularly the  $\lambda_1$ ,  $\lambda_2$  and  $\lambda_3$ .<sup>33</sup> Future studies with improved data acquisition parameters are needed to validate and extend our findings. Second, the automated TBSS methodology is subject to bias, especially in areas of tract junctions or crossing fibers, such as the superior and inferior longitudinal fasciculus. Therefore, the interpretations of the diffusion changes in these regions must be interpreted with caution. Third, we only focused on the WM changes in NMO patients in this study. The relationship between these functional and structural changes, however, is still unclear. In future studies, the putative connection between WM degeneration and functional connectivity could be examined by combining both DTI and fMRI techniques. Fourth, the NMO-IgG test, which is part of the diagnostic criteria for NMO, was not available in our study, but in future it will be very interesting for us to replicate and extend these results also focusing on subgroups based on NMO-IgG testing, although this will require recruitment of additional cohorts of patients. Finally, the exact histopathological processes leading to changes in DTI eigenvalues are complex, and appropriate animal models where MRI DTI assessments can be directly correlated with morphometric histology will be very useful.

### Conclusion

We used the DTI technique and TBSS method to investigate changes in both the anisotropic properties of diffusion (FA) and absolute diffusivities (MD,  $\lambda_1$  and  $\lambda_{23}$ ) in NMO patient cerebral WM tracts, and provide imaging evidence for widespread cerebral WM DTI abnormalities. While

these findings require independent replication, they potentially signify the presence of widespread, low-grade cerebral pathology in NMO.

### Funding

Dr Yaou Liu was supported by McDonald Fellowship from Multiple Sclerosis International Federation (MSIF). This work was supported by the National Science Foundation of China (grant numbers 81101038, 81000633 30930029, 30800267, 30870667 and 81030028).

### References

1. Wingerchuk DM, Lennon VA, Pittock SJ, Lucchinetti CF and Weinschenker BG. Revised diagnostic criteria for neuromyelitis optica. *Neurology* 2006; 66: 1485–1489.
2. Wingerchuk DM, Lennon VA, Lucchinetti CF, Pittock SJ and Weinschenker BG. The spectrum of neuromyelitis optica. *Lancet Neurol* 2007; 6: 805–815.
3. Filippi M, Rocca MA, Momiola L, et al. MRI and magnetization transfer imaging changes in the brain and cervical cord of patients with Devic's neuromyelitis optica. *Neurology* 1999; 53: 1705–1710.
4. Pittock SJ, Lennon VA, Krecke K, Wingerchuk DM, Lucchinetti CF and Weinschenker BG. Brain abnormalities in neuromyelitis optica. *Arch Neurol* 2006; 63: 390–396.
5. Bichueti DB, Rivero RL, de Oliveira EM, et al. White matter spectroscopy in neuromyelitis optica: a case control study. *J Neurol* 2008; 255: 1895–1899.
6. Yu CS, Lin FC, Li KC, et al. Diffusion tensor imaging in the assessment of normal-appearing brain tissue damage in relapsing neuromyelitis optica. *AJNR Am J Neuroradiol* 2006; 27: 1009–1015.
7. Yu C, Lin F, Li K, et al. Pathogenesis of normal-appearing white matter damage in neuromyelitis optica: diffusion-tensor MR imaging. *Radiology* 2008; 246: 222–228.
8. Rocca MA, Agosta F, Mezzapesa DM, et al. Magnetization transfer and diffusion tensor MRI show gray matter damage in neuromyelitis optica. *Neurology* 2004; 62: 476–478.
9. Rovaris M, Gass A, Bammer R, et al. Diffusion MRI in multiple sclerosis. *Neurology* 2005; 65: 1526–1532.
10. Acosta-Cabronero J, Williams GB, Pengas G and Nestor PJ. Absolute diffusivities define the landscape of white matter degeneration in Alzheimer's disease. *Brain* 133: 529–539.
11. Beaulieu C. The basis of anisotropic water diffusion in the nervous system - a technical review. *NMR Biomed* 2002; 15: 435–455.
12. Song SK, Sun SW, Ramsbottom MJ, Chang C, Russell J and Cross AH. Demyelination revealed through MRI as increased radial (but unchanged axial) diffusion of water. *Neuroimage* 2002; 17: 1429–1436.
13. Song SK, Yoshino J, Le TQ, et al. Demyelination increases radial diffusivity in corpus callosum of mouse brain. *Neuroimage* 2005; 26: 132–140.
14. Sun SW, Liang HF, Schmidt RE, Cross AH and Song SK. Selective vulnerability of cerebral white matter in a murine model of multiple sclerosis detected using diffusion tensor imaging. *Neurobiol Dis* 2007; 28: 30–38.
15. Wu Q, Butzkueven H, Gresle M, et al. MR diffusion changes correlate with ultra-structurally defined axonal degeneration in murine optic nerve. *Neuroimage* 2007; 37: 1138–1147.

16. Smith SM, Jenkinson M, Johansen-Berg H, et al. Tract-based spatial statistics: voxelwise analysis of multi-subject diffusion data. *Neuroimage* 2006; 31: 1487–1505.
17. Douaud G, Smith S, Jenkinson M, et al. Anatomically related grey and white matter abnormalities in adolescent-onset schizophrenia. *Brain* 2007; 130: 2375–2386.
18. Karlsgodt KH, van Erp TG, Poldrack RA, Bearden CE, Nuechterlein KH and Cannon TD. Diffusion tensor imaging of the superior longitudinal fasciculus and working memory in recent-onset schizophrenia. *Biol Psychiatry* 2008; 63: 512–518.
19. Cader S, Johansen-Berg H, Wylezinska M, et al. Discordant white matter N-acetylaspartate and diffusion MRI measures suggest that chronic metabolic dysfunction contributes to axonal pathology in multiple sclerosis. *Neuroimage* 2007; 36: 19–27.
20. Kurtzke JF. Rating neurologic impairment in multiple sclerosis: an expanded disability status scale (EDSS). *Neurology* 1983; 33: 1444–1452.
21. Blanc F, Zephir H, Lebrun C, et al. Cognitive functions in neuromyelitis optica. *Arch Neurol* 2008; 65: 84–88.
22. Sabater L, Giral A, Boronat A, et al. Cytotoxic effect of neuromyelitis optica antibody (NMO-IgG) to astrocytes: an in vitro study. *J Neuroimmunol* 2009; 215: 31–35.
23. Bradl M, Misu T, Takahashi T, et al. Neuromyelitis optica: pathogenicity of patient immunoglobulin in vivo. *Ann Neurol* 2009; 66: 630–643.
24. Parratt JD and Prineas JW. Neuromyelitis optica: a demyelinating disease characterized by acute destruction and regeneration of perivascular astrocytes. *Mult Scler* 16: 1156–1172.
25. Takano R, Misu T, Takahashi T, Sato S, Fujihara K and Itoyama Y. Astrocytic damage is far more severe than demyelination in NMO: a clinical CSF biomarker study. *Neurology* 75: 208–216.
26. Pierpaoli C and Basser PJ. Toward a quantitative assessment of diffusion anisotropy. *Magn Reson Med* 1996; 36: 893–906.
27. Pierpaoli C, Barnett A, Pajevic S, et al. Water diffusion changes in Wallerian degeneration and their dependence on white matter architecture. *Neuroimage* 2001; 13: 1174–1185.
28. Song SK, Sun SW, Ju WK, Lin SJ, Cross AH and Neufeld AH. Diffusion tensor imaging detects and differentiates axon and myelin degeneration in mouse optic nerve after retinal ischemia. *Neuroimage* 2003; 20: 1714–1722.
29. Beaulieu C, Does MD, Snyder RE and Allen PS. Changes in water diffusion due to Wallerian degeneration in peripheral nerve. *Magn Reson Med* 1996; 36: 627–631.
30. Anjari M, Srinivasan L, Allsop JM, et al. Diffusion tensor imaging with tract-based spatial statistics reveals local white matter abnormalities in preterm infants. *Neuroimage* 2007; 35: 1021–1027.
31. Burzynska AZ, Preuschhof C, Backman L, et al. Age-related differences in white matter microstructure: region-specific patterns of diffusivity. *Neuroimage* 49: 2104–2112.
32. Makris N, Kennedy DN, McInerney S, et al. Segmentation of subcomponents within the superior longitudinal fascicle in humans: a quantitative, in vivo, DT-MRI study. *Cereb Cortex* 2005; 15: 854–869.
33. Huisman TA, Loenneker T, Barta G, et al. Quantitative diffusion tensor MR imaging of the brain: field strength related variance of apparent diffusion coefficient (ADC) and fractional anisotropy (FA) scalars. *Eur Radiol* 2006; 16: 1651–1658.